Science Advances
AAAS

advances.sciencemag.org/cgi/content/full/4/8/eaat1115/DC1

Supplementary Materials for

Current-induced dynamics of skyrmion strings

T. Yokouchi*, S. Hoshino, N. Kanazawa, A. Kikkawa, D. Morikawa, K. Shibata, T. Arima, Y. Taguchi, F. Kagawa, N. Nagaosa, Y. Tokura*

*Corresponding author. Email: yokouchi@cmr.t.u-tokyo.ac.jp (T.Y.); tokura@riken.jp (Y.T.)

Published 10 August 2018, *Sci. Adv.* **4**, eaat1115 (2018)
DOI: 10.1126/sciadv.aat1115

This PDF file includes:

Section S1. Determination of magnetic phase diagram for MnSi thin plate
Section S2. Relationship between nonreciprocal nonlinear Hall effect and second-harmonic resistivity
Section S3. Current dependence of nonlinear Hall effect measured by using square-wave current
Section S4. Frequency dependence of skyrmion velocity
Section S5. Calculation of nonreciprocal nonlinear Hall responses to AC
Section S6. Calculation of current-induced dynamics of a single skyrmion string
Fig. S1. Functional forms of the dimensionless functions $f_b(\lambda)$ and $f_e(\lambda)$.
Fig. S2. Temperature dependence of longitudinal resistivity and magnetic field dependence of planar Hall resistivity.
Fig. S3. Current dependence of nonreciprocal nonlinear Hall effect measured by using square-wave current.
Fig. S4. Frequency dependence of skyrmion velocity.
References (*32*–*34*)

Section S1. Determination of magnetic phase diagram for MnSi thin plate

We determined the magnetic phase diagram for MnSi thin plate from the measurements of longitudinal resistivity (ρ_{xx}) and planar Hall resistivity (ρ^{PHE}), both of which are widely employed as the sensitive probes of magnetic transitions in MnSi (*8*, *32*). The helical-ordering temperature (T_c) at the zero magnetic field is determined as the temperature where the ρ_{xx}-T curve exhibits an inflection (fig. S2A). The helical-to-conical, helical/conical-to-skyrmion, and conical-to-ferromagnetic transitions are determined from the kinks in B-dependence of ρ^{PHE} (fig. S2 B-E).

Section S2. Relationship between nonreciprocal nonlinear Hall effect and second-harmonic resistivity

In this section we describe the relationship among (1) the nonreciprocal nonlinear Hall effect, which is discussed on the basis of a symmetry argument, (2) the second-harmonic resistivity, which we experimentally measured as shown in the main text and (3) the DC limit of nonreciprocal nonlinear Hall resistivity, which we calculated theoretically.

From the viewpoint of symmetry, the finite nonreciprocal nonlinear Hall voltage ${V_z}^{\mathrm{Non}}$ in MnSi can appear in the experimental setup of Fig. 1A in the main text, and is described in the following expression

$$ {V_z}^{\mathrm{Non}} = E_z d = \alpha(j_x, B_z) j_x d $$

The $\alpha(j_x, B_z)$ is the nonreciprocal nonlinear Hall coefficient, being pseudo-scalar and an odd function of both j_x and B_z. Here d is distance between voltage terminals (see also Fig. 1A in the main text for the definition of the x-y-z coordinate).

The relationship between the nonreciprocal nonlinear Hall effect and experimentally-observed second harmonic Hall resistivity is derived as follows. When we input sine-wave current $j_x = j_{0x}\sin(2\pi ft)$, the nonreciprocal nonlinear Hall voltage ${V_z}^{\mathrm{Non}}$ can be described by a series of $\cos(2\pi nft)$ and $\sin(2\pi nft)$

$$ {V_z}^{\mathrm{Non}} = \alpha(j_x, B_z) j_x d = \sum_{n=0} [A_{\mathrm{n}}(j_{0x}, B_z)\cos(2\pi nft) + B_{\mathrm{n}}(j_{0x}, B_z)\sin(2\pi nft)] d $$

Here, the coefficients of $\cos(4\pi ft)$ and $\sin(4\pi ft)$ are real and imaginary parts of second harmonic Hall voltage ($\mathrm{Re}V_z^{2f}$ and $\mathrm{Im}V_z^{2f}$), respectively. We therefore obtain

$$ \mathrm{Re}V_z^{2f} = A_2(j_{0x}, B_z) d $$

$$ \mathrm{Im}V_z^{2f} = B_2(j_{0x}, B_z) d $$

We define the real and imaginary parts of second harmonic resistivity as

$$ \mathrm{Re}\rho_{zx}^{2f} = \frac{\mathrm{Re}V_z^{2f}}{j_{0x}\, d} = A_2(j_{0x}, B_z)/j_{0x} $$

$$ \mathrm{Im}\rho_{zx}^{2f} = \frac{\mathrm{Im}V_z^{2f}}{j_{0x}\, d} = B_2(j_{0x}, B_z)/j_{0x} $$

In the theoretical part, we calculate the DC limit of nonreciprocal nonlinear Hall resistivity [$\propto A_0(j_{0x}, B_z)$], not second harmonic Hall resistivity [$\propto A_2(j_{0x}, B_z)$]. Here we note $A_2(j_{0x}, B_z)$ should asymptotically approach $A_0(j_{0x}, B_z)$ in the low-frequency limit.

Section S3. Current dependence of nonlinear Hall effect measured by using square-wave current

As mentioned in the main text, in order to avoid increase in the sample temperature due to the Joule heating, we controlled the cooling power based on the feedback from the simultaneous monitoring of the longitudinal resistivity. However, there is a possibility that temporal change of the sample temperature occurs due to the sine-wave input current. As illustrated in fig. S3A, when sine-wave current $j_x \sin(2\pi f t)$ is applied, the Joule heating is proportional to $\sin^2(2\pi f t)$. If the thermal relaxation time of samples is much faster than one cycle of sine-wave current, the sample temperature decreases around the nodes of the sine-wave current.

To rule out the influence of temporal temperature change, we additionally measured current dependence of nonreciprocal nonlinear Hall effect by using a square-wave current, which generates time-independent Joule heating (see fig. S2B). When a square-wave current applied, the nonlinear Hall voltage appears as a constant DC voltage V_z^{DC} parallel to magnetic field. Here we define nonreciprocal nonlinear Hall resistivity measured by using the square-wave current as $\rho_{zx}^{\mathrm{square}} = V_z^{\mathrm{DC}}/(j_x d)$. As in the case of the measurement using the sine-wave current, we estimated the sample temperature from the longitudinal resistivity, and adjusted the temperature of the heat bath of PPMS to control the cooling power. As shown in fig. S3C the sample temperature stays almost constant. As shown in fig. S3D, the current dependence of $\rho_{zx}^{\mathrm{square}}$ in the skyrmion phase exhibits a profile almost similar to that of second harmonic Hall resistivity measured by using the sine-wave current (Fig. 3B in the main text). This result rules out the possibility that the non-monotonous current dependence of second-harmonic Hall resistivity measured by using the sine-wave current results from the possible temporal temperature change.

Section S4. Frequency dependence of skyrmion velocity

In this section, we discuss the dependency of skyrmion velocity ($\boldsymbol{v}_{\mathrm{Sk}}$) on driving current frequency by using the Thiele's equations (*33*, *34*)

$$m\frac{d\boldsymbol{v}_{\mathrm{Sk}}}{dt} + \boldsymbol{G} \times (\boldsymbol{v}_{\mathrm{Sk}} - \boldsymbol{v}_{\mathrm{e}}) + D\alpha\boldsymbol{v}_{\mathrm{Sk}} = 0$$

Here, m, D, α and $\boldsymbol{v}_{\mathrm{e}}$ are effective mass of skyrmion, dissipative force constant, the Gilbert damping coefficient, and drift velocity of electrons, respectively. We have neglected the so-called β term, which describes non-adiabatic effect, since the magnitude of β is small in MnSi (*11*). In addition, the skyrmion velocity almost independents of the magnitude of β (*13*). The gyromagnetic coupling vector $\boldsymbol{G}$ is given by $\boldsymbol{G} = (0,0,G)$ with $G = 4\pi N_{\mathrm{Sk}}$ being proportional to skyrmion number N_{Sk} . In the moving regime, we can treat the impurity potential perturbatively. We ignore a pinning force in Thiele equation to keep the leading-order contribution because we measured the frequency dependence of second-harmonic resistivity with relatively large current density compared to the critical current density ($j \sim 2j_{\mathrm{c}}$) for moving skyrmions. The frequency dependence of skyrmion velocity along the current direction (v_{Sk}^{x}) is derived as follows

$$v_{\mathrm{Sk}}^{x}(f) = \frac{\dfrac{G}{G^2 + (D\alpha)^2}}{1 + 2\pi i \dfrac{2mD\alpha}{G^2 + (D\alpha)^2} f} v_{\mathrm{e}}$$

Here because the skyrmion velocity perpendicular to the current direction (v_{Sk}^{y}) is smaller than v_{Sk}^{x}, we ignore v_{Sk}^{y}; when we ignore the β term, the ratio between v_{Sk}^{x} and v_{Sk}^{y} is described as $v_{\mathrm{sk}}^{x}/v_{\mathrm{sk}}^{y} = G/\alpha D$ (*13*). Using the typical parameter in metals: $\alpha = 0.04, D = 5.57\pi, G = 4\pi$ (*13*), we obtain $v_{\mathrm{Sk}}^{x}/v_{\mathrm{Sk}}^{y} = G/\alpha D$ = 18.0. Therefore the skyrmion velocity is almost parallel to the current direction. As shown in fig. S4, the real

part of $v_{\mathrm{Sk}}^{x}(f)$ begins to decrease around $f = \frac{G^2+(D\alpha)^2}{4\pi mD\alpha}$, and the imaginary part of $v_{\mathrm{Sk}}^{x}(f)$ exhibits the peak at $f = \frac{G^2+(D\alpha)^2}{4\pi mD\alpha}$. This is because skyrmions motion cannot follow the driven AC current with frequency above $f = \frac{G^2+(D\alpha)^2}{4\pi mD\alpha}$. The frequency profile of skyrmion velocity resembles that of second-harmonic resistivity (Fig. 3D in the main text), which supports the relationship of nonreciprocal nonlinear Hall signal to translational motion of SkL.

Section S5. Calculation of nonreciprocal nonlinear Hall responses to AC

While the DC component becomes finite only for the fourth-order contribution with respect to impurity potentials, the AC component can be finite already for the second-order term of impurity potentials. However, this quantity is not relevant to the one observed in experiments. To see this, let us first look at the explicit form of the expression. Here, for simplicity of theoretical expressions, we take the random-Ising magnetic field for the impurity potential: $H_{\mathrm{imp}} = \int \frac{d\boldsymbol{r}}{\ell^3} V(\boldsymbol{r}) n^z$, whose conclusion is applied also to the random anisotropy considered in the main text. Under the AC current, the position of skyrmion crystal has the form $\boldsymbol{R}(t) = \boldsymbol{R}_0 \sin\omega_0 t$, and we then derive

$$
\begin{aligned}
E_z^{\mathrm{AC}}(t) &= \int \frac{d\boldsymbol{r}}{\Omega} Pe_z(\boldsymbol{r}, t) \\
&= \frac{2Pb_z V_{\mathrm{imp}}^2 a^6}{3Q^2\ell^3} \sum_{ijk} \int \frac{d\boldsymbol{q}}{(2\pi)^3} \sum_{M,N=-\infty}^{\infty} E_{ij} M\omega_0 q_z \left[1+(-1)^{M+N}\right] e^{-i(M+N)\omega_0 t} \\
&\quad \times J_M(\boldsymbol{Q}_k \cdot \boldsymbol{R}_0) J_N(\boldsymbol{Q}_k \cdot \boldsymbol{R}_0) G_{ik}(\boldsymbol{q}, M\omega_0) G_{jk}(-\boldsymbol{q}, N\omega_0) + O(V_{\mathrm{imp}}^4)
\end{aligned}
$$

where $J_N(x)$ is the Bessel function of the first kind. We note that the contribution from emergent magnetic field perpendicular to external field vanishes in the uniform limit. From this expression it is clear that $E_z^{\mathrm{AC}}(t)$ has only the components with the frequency $\omega = 0, \pm 2\omega_0, \pm 4\omega_0, \cdots$. However, this is an irrelevant contribution to the quantity measured by experiments, since $E_z^{\mathrm{AC}}(t)$ has finite value only when the frequency $\hbar\omega_0$ is

comparable to $\frac{D^2}{J}$, which is the characteristic energy scale for chiral magnets and is the order of gigahertz. In the experiments, the used frequency ω_0 $(= 2\pi f)$ is much lower than this value ($f \simeq 10$Hz), and even in the DC case the signal has been captured. Furthermore, a fast oscillation of the electrical current cannot be followed by the motion of spin texture, as shown in Fig. 3D of main text. Thus the contribution from second-order of impurity potentials is likely to be dropped from experimental observations, and we need to consider the higher-order terms as discussed in main text.

Section S6. Calculation of current-induced dynamics of a single skyrmion string

As described in the main text, for an intuitive understanding of the dynamics of the skyrmion string, we focus on dynamics of a single skyrmion string. In this section, we describe the detailed calculation method of dynamics of a skyrmion string and emergent electromagnetic field. The position $\boldsymbol{R}(z,t)$ of a flowing single skyrmion string along magnetic field direction (z) is described by $\boldsymbol{R} = \boldsymbol{v}_{\mathrm{Sk}} t + z\hat{\boldsymbol{z}} + \boldsymbol{u}$ where the vector $\boldsymbol{u}(z,t) = (u_x, u_y, 0)$ and $\boldsymbol{v}_{\mathrm{Sk}}$ ($\parallel \hat{\boldsymbol{x}}$) are the displacement field and the skyrmion velocity, respectively. The emergent magnetic and electric fields are then written as (*30*)

$$\boldsymbol{b} = \frac{b_1 \partial_z \boldsymbol{R}}{|\partial_z \boldsymbol{R}|} = \frac{b_1 \left(\partial_z u_x, \partial_z u_y, 1\right)}{\sqrt{1 + (\partial_z u_x)^2 + \left(\partial_z u_y\right)^2}} \tag{S1}$$

$$\boldsymbol{e} = -\partial_t \boldsymbol{R} \times \boldsymbol{b} \tag{S2}$$

where b_1 is an emergent magnetic flux density for the single skyrmion string.
We describe a bending of the skyrmion string as a wave packet constructed by superposition of eigenmodes of the dispersion of the low-energy excitation $\epsilon(\boldsymbol{q})$

$$u_x(z,t) = C_1 \left[\int dq_z e^{-(q_z - q_1)^2/\sigma^2} + \int dq_z e^{-(q_z - q_2)^2/\sigma^2} \right] \cos(\omega t - q_z z) e^{-gt} \tag{S3}$$

$$u_y(z,t) = C_2\left[\int dq_z e^{-(q_z-q_1)^2/\sigma^2} + \int dq_z e^{-(q_z-q_2)^2/\sigma^2}\right]\sin(\omega t - q_z z)e^{-gt} \quad \text{(S4)}$$

Here, $\hbar\omega$ is equal to $\epsilon(\boldsymbol{q})$, and q_1 and q_2 are solutions of the equation $\epsilon(\boldsymbol{q}) = \epsilon_0$, where ϵ_0 is the energy of driving electric current (see also Fig. 4A). The g and σ are a damping for the skyrmion string and a standard deviation of the Gaussian function. The constants C_1 and C_2 describe the magnitude of bending of skyrmion strings. We calculated emergent magnetic and electric filed by inserting Eq. S3 and S4 into Eq. S1 and S2. (See Fig. 4. D, E, G, H in the main text for the result of calculations).

We note that, in the case of the single string picture, the nonreciprocal nonlinear Hall electric field in the spatially uniform and DC-limit is given by

$$E_z^{\mathrm{DC,string}} = \frac{Pb_1}{2}\sum_{\mu\nu\rho}\epsilon_{\mu\nu z}\lim_{T\to\infty}\int_{-T}^{T}\frac{dt}{2T}\int\frac{dz}{L_z}\left[-(\boldsymbol{v}_e - \boldsymbol{v}_{\mathrm{Sk}})_\mu + \partial_t u_\mu\right]\partial_z u_\nu\left(\partial_z u_\rho\right)^2$$

with a system size L_z along z-direction. Here we have kept the leading-order contributions for E_z^{DC}. As in the case of DC limit calculated in SkL (see the main text and the method section), the leading-order contribution of $E_z^{\mathrm{DC,\ string}}$ is also third- and fourth-order terms with respect to the internal deformation field variables.

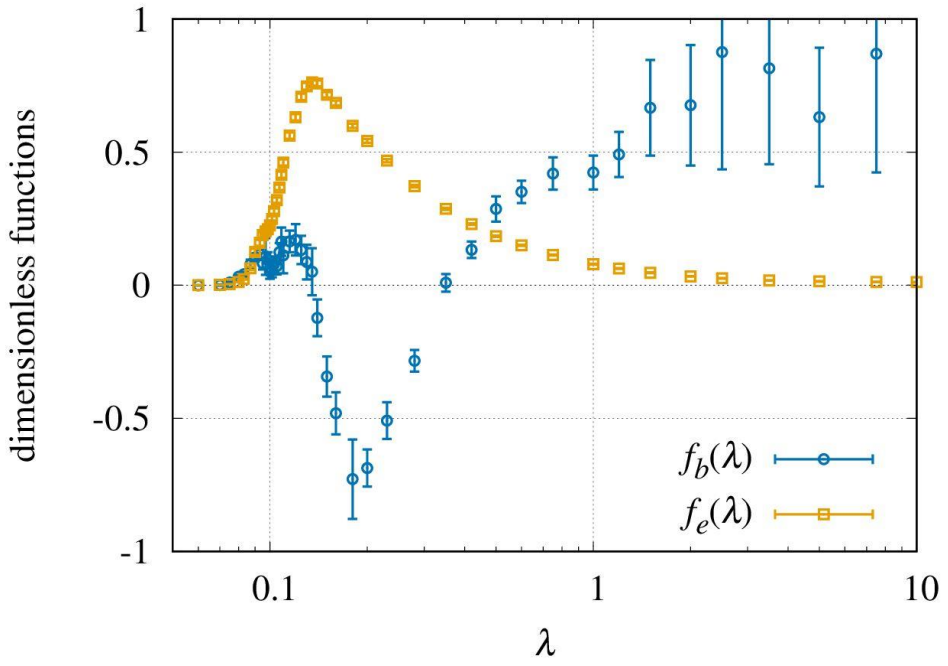

Fig. S1. Functional forms of the dimensionless functions $f_b(\lambda)$ and $f_e(\lambda)$. The wave-vector integrals to evaluate $f_{b,e}(\lambda)$ have been performed by the Monte Carlo method, and the error bars represent a standard error.

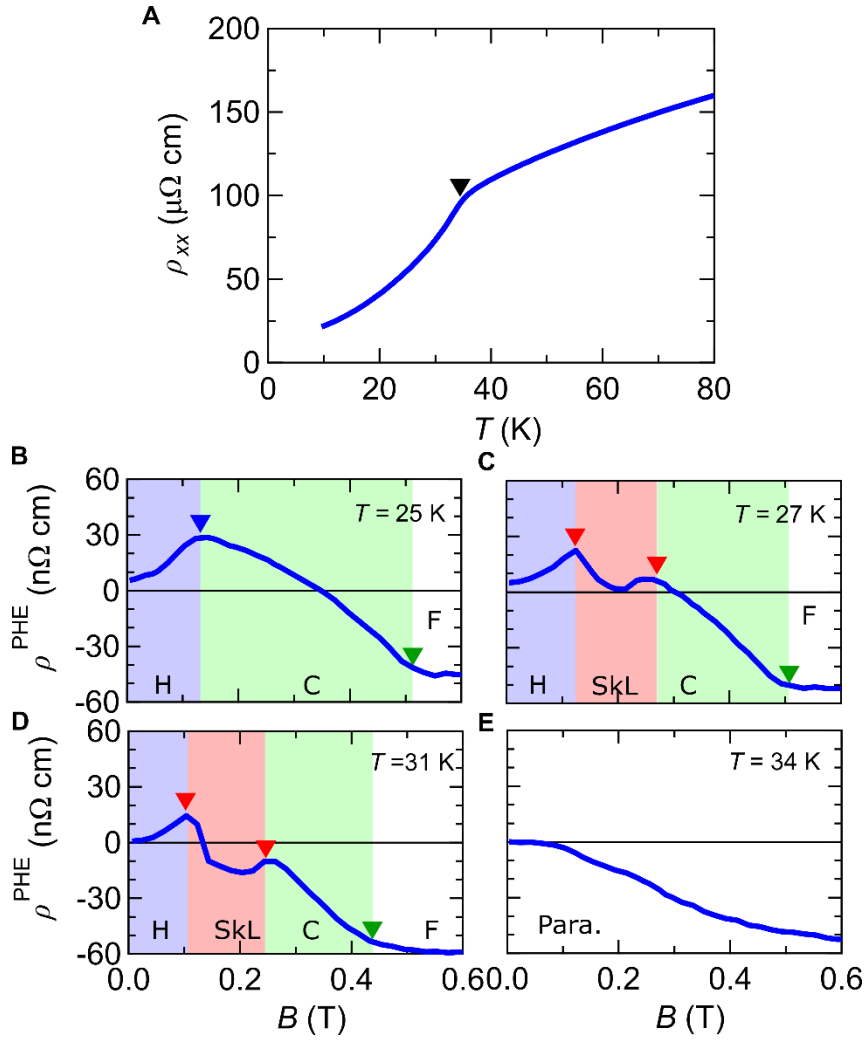

Fig. S2. Temperature dependence of longitudinal resistivity and magnetic field dependence of planar Hall resistivity. (**A**) Temperature (T) dependence of longitudinal resistivity (ρ_{xx}). We determined the helical-ordering temperature as the inflection point of the $\rho_{xx} - T$ curve (the black triangle). (**B-E**) Magnetic-field (B) dependence of planar Hall resistivity (ρ^{PHE}) at various temperatures. We assigned the kinks in B-dependence of ρ^{PHE} to the helical-to-conical transition (the blue triangle), helical/conical-to-skyrmion transition (the red triangles), and conical-to-ferromagnetic transition (the green triangles). The letters H, C, SkL, and F represent helical, conical, skyrmion-lattice, and ferromagnetic phases, respectively.

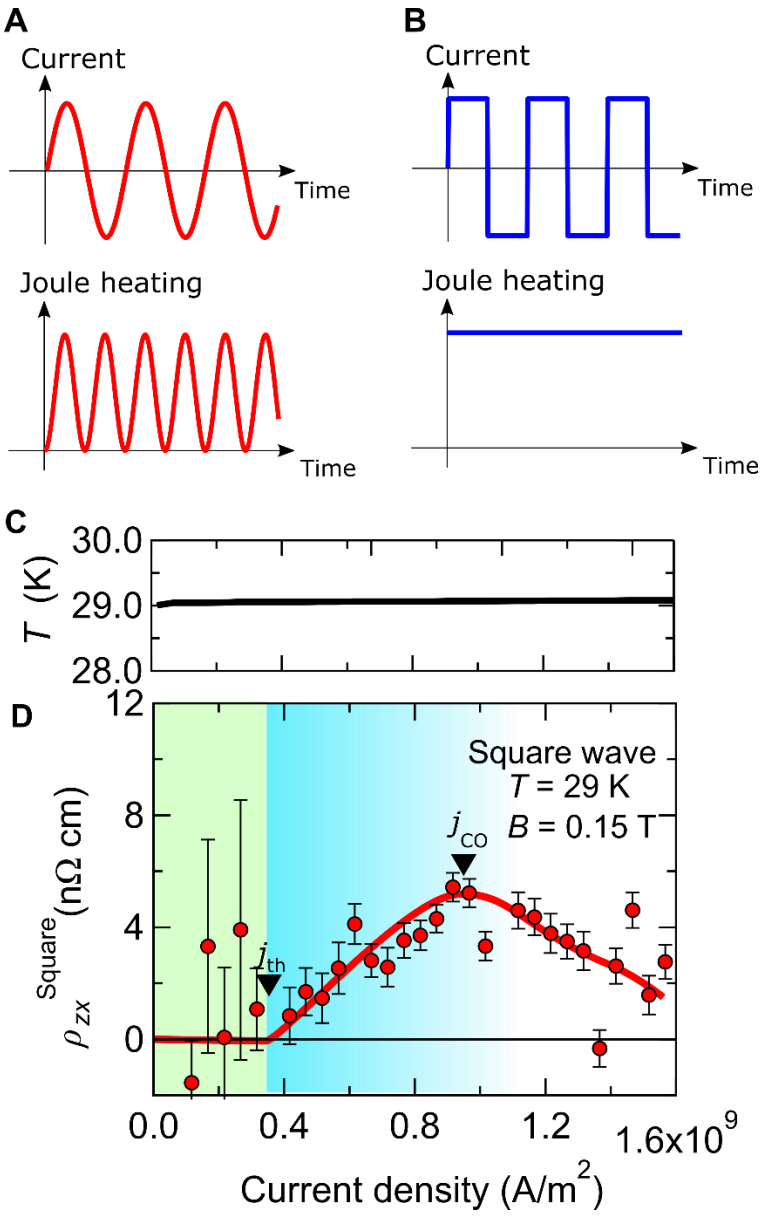

Fig. S3. Current dependence of nonreciprocal nonlinear Hall effect measured by using square-wave current. (**A** and **B**) Schematic illustrations of time profiles of the sine-wave (A) and square-wave (B) input currents, and those of their corresponding Joule heating. (**C** and **D**) The current dependence of sample temperature estimated from the longitudinal resistivity measurement (C) and nonlinear Hall effect measured using square-wave current (D).

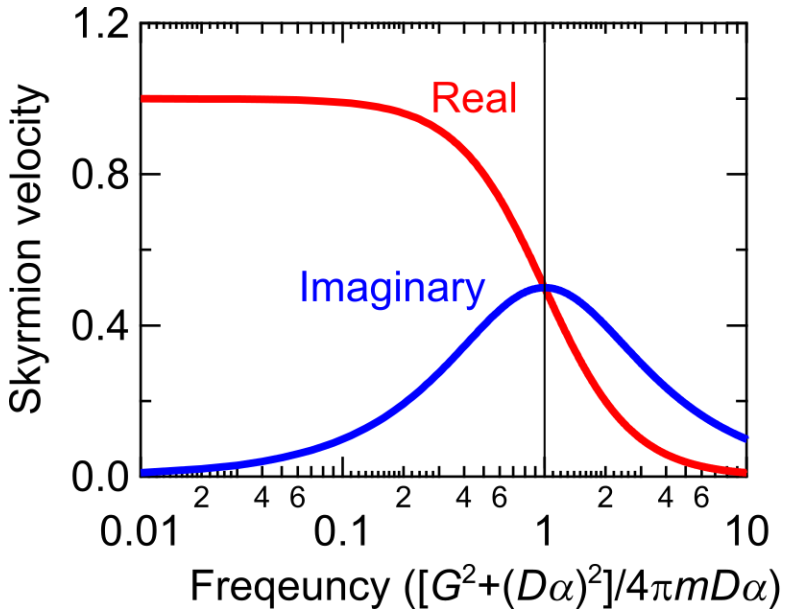

Fig. S4. Frequency dependence of skyrmion velocity. The real part (red) and imaginary part (blue) of frequency-dependent skyrmion velocity derived from Thiele's equation. The vertical and horizontal axes are normalized by the velocity at zero frequency and $\frac{G^2+(D\alpha)^2}{4\pi mD\alpha}$, where *G*, *D*, α and m are gyromagnetic coupling, dissipative force, the coefficients for Gilbert damping, and effective mass of skyrmion, respectively.